Biocompatibility of submicron Bioglass® powders obtained by a top-down approach

ARTICLE *in* JOURNAL OF BIOMEDICAL MATERIALS RESEARCH PART B APPLIED BIOMATERIALS · JULY 2014

Impact Factor: 2.76 · DOI: 10.1002/jbm.b.33076

Society For Biomaterials

Biocompatibility of submicron Bioglass® powders obtained by a top-down approach

Anja Dörfler,[1]*† Rainer Detsch,[1]* Stefan Romeis,[2]* Jochen Schmidt,[2] Claudia Eisermann,[2] Wolfgang Peukert,[2] Aldo R. Boccaccini[1]

[1]Friedrich-Alexander-University Erlangen-Nuremberg, Institute of Biomaterials (WW 7), Cauerstraße 6, 91058 Erlangen, Germany

[2]Friedrich-Alexander-University Erlangen-Nuremberg, Institute of Particle Technology (LFG), Cauerstraße 4, 91058 Erlangen, Germany

Received 19 July 2013; revised 9 October 2013; accepted 29 October 2013
Published online 00 Month 2013 in Wiley Online Library (wileyonlinelibrary.com). DOI: 10.1002/jbm.b.33076

Abstract: In this study *in vitro* bioactivity and biocompatibility of two submicron 45S5 Bioglass® powders obtained by top-down processing have been evaluated and are compared to the as-received powder. Both submicron powders exhibited flake-like morphologies with lateral extensions of only a few microns; the flake thickness accounted for a few tens of nanometers. Enhanced *in vitro* bioactivity was found for the comminuted powders upon immersion in simulated body fluid. *In vitro* biocompatibility was evaluated by incubation of MG-63 osteoblast-like cells with various amounts (0–200 μg/mL) of the glass powders. Neither LDH-activity nor mitochondrial activity (WST-8) tests indicated cell toxicity. Increased mitochondrial activity was found for the submicron powders: incubation with high amounts revealed up to a threefold increase of osteoblast activity (ALP-activity). An overgrowth of the formed mineralized phase with phenotypical MG-63 cells was found by staining only for the submicron glasses. A distance ring is formed for the as-received powder. Superior bioactivity markers are found for shorter process times, that is, lower mass specific surface areas. This is attributed to the formation of carbonates during the comminution process. © 2013 Wiley Periodicals, Inc. J Biomed Mater Res Part B: Appl Biomater 00B: 000–000, 2013.

Key Words: 45S5 Bioglass®, top-down production, submicron particles, in vitro bioactivity and biocompatibility, MG-63 cells

How to cite this article: Dörfler A, Detsch R, Romeis S, Schmidt J, Eisermann C, Peukert W, Boccaccini AR. 2013. Biocompatibility of submicron Bioglass® powders obtained by a top-down approach. J Biomed Mater Res Part B 2013:00B:000–000.

INTRODUCTION

Several glass compositions are known to be bioactive when in contact with biologic environments.[1,2] The most prominent example is 45S5 Bioglass® (45S5BG) from the quaternary Na_2O-CaO-P_2O_5-SiO_2 glass forming system.[3] This Class A[1,4] bioactive glass (BG) is capable of forming a strong bonding to surrounding soft[5] and hard tissue.[6] A proposed mechanism leading to tissue bonding postulates a material based sequence and parallel steps occurring on the cellular level.[1,4,7] In contact to physiological fluids, the glass surface releases network modifiers and silica species. Silica is genetically active on the cellular level and stimulates mitosis of osteoprogenitor cells[8] as well as angiogenesis.[9] A silica layer on top of the glass is formed and adsorbs Ca^{2+} and PO_4^{3-} from the surrounding biological fluid; the local supersaturation with respect to carbonated hydroxyapatite is increased and precipitation of bone-like carbonated hydroxyapatite (HCAp) occurs. Partially in parallel, the adsorption of proteins, the attachment of cells, the differentiation of stem cells into osteoblasts, and finally the formation of a mineralized extracellular matrix are suggested to take place. The formation of the HCAp layer is deemed as a prerequisite for bioactivity;[10–12] Kokubo et al.[13,14] developed an *in vitro* test assessing bioactivity by *in vitro* formation of a HCAp layer upon immersion in simulated body fluid (SBF).

Currently, mainly melt-derived BGs are applied in the form of particulates with sizes in the upper micrometer size range. Either the particulates are applied directly or are further processed into small bulky implants.[2,7] Recently, applications as scaffolds in bone tissue engineering[15] and active fillers in composites are investigated.[16]

Several recent studies indicate enhanced bioactive properties of submicron and nanoscaled BG (nBG), including accelerated HCAp formation,[17] a more rapid release of ionic species and dentin mineralization[18] as well as enhanced disinfecting properties.[19] There are many potential applications

*These authors contributed equally and share the first authorship for this article.
†Present address: Sandoz International GmbH, Industriestraße 25, 83607 Holzkirchen, Germany
Correspondence to: A. R. Boccaccini (e-mail: aldo.boccaccini@ww.uni-erlangen.de)
Contract grant sponsor: Emerging Fields Initiative supported "TOPbiomat" project of the University of Erlangen-Nuremberg (to A.D., R.D., and A.R.B.), German Science Foundation within the Leibniz program (to S.R., J.S., C.E., and W.P.), and Cluster of Excellence "Engineering of Advanced Materials"

for nBGs, for example, wound dressings,[20] tissue engineering applications,[7,21,22] and their usage as active filler in hydrogels or collagen and polymer matrix composites.[23–25] However, a series of limitations still needs to be overcome: commonly employed bottom-up processing routes[26,27] toward nBGs may be complex, cost- and energy intensive, and often difficult to handle, toxic precursor substances are needed. On the other hand, stirred media milling is a simple, versatile and scalable method to produce a large variety of micron and nanosized powders.[28–30] Recently, Romeis et al.[31] comminuted a melt-derived 45S5BG in a stirred media mill and obtained submicron particles of enhanced *in vitro* bioactivity. Biocompatibility and the response of cells to these new particles have not been tested yet.

In the present study *in vitro* bioactivity and biocompatibility of two submicron powders, obtained from wet comminution for 5 h and 24 h using *n*-pentanol as solvent of a commercial 45S5BG are investigated. The as-received glass was used as a reference material. Bioactivity was judged by SBF immersion; biocompatibility and the response of cells to these new materials were evaluated by incubation of MG-63 cells with various powder amounts (up to 200 μg/mL). LDH-activity, mitochondrial activity, and osteoblast activity (ALP-activity) were assessed as markers for biocompatibility. Cell morphology was evaluated by light microscopy and after staining by fluorescence microscopy.

EXPERIMENTAL PROCEDURE

Comminution of 45S5 Bioglass®

Briefly, the laboratory stirred media mill PE075 (Netzsch) was used to process a 3 wt % of 45S5BG containing *n*-pentanol (>98.0%, VWR) suspension. Approximately 1.8 kg Yttrium-stabilized zirconia beads (2 mm diameter, Tosho) were used. Tip speed of the three disc stirrer was set to 4.9 m/s (1500 rpm). Suspensions were removed after 5 h (BG10) and 24 h (BG30). Powder recovery was done by centrifugation (10 min, 14000 rpm, Centrifuge 5418, Eppendorf) and subsequent drying (160°C, 24 h, muffle furnace, Nabertherm). To eliminate an influence of exposure time to the solvent, the BG10 suspension was stored for 19 h before drying.

Powder analysis

Nitrogen sorption (Nova4200e, Quantachrome). Nitrogen sorption was performed after sample degassing (2 h, 250°C, $p < 10^{-2}$ torr) at liquid nitrogen temperature. Mass-specific surface areas (S_m) were obtained according to BET theory (five points; p/p_0 0.02–0.35).[32]

Microwave Digestion (Multiwave 3000, Anton Paar). Approximately 0.02 g of powder were microwave digested (90 min, 800 W) for ICP-OES analyses. The digestion solution was: 2 mL hydrofluoric acid (48%, supra purity), 2 mL nitric acid (69%, supra purity) and 4 mL hydrochloric acid (35%, supra purity). After digestion 2 g boric acid (>99.8%) dissolved in 40 mL deionized water was added and the total volume was set to 250 mL. All chemicals were obtained from Carl Roth.

ICP-OES analyses (Optima 8300, Perkin Elmer). The digested sample solutions were fed with a flow rate of 1.8 mL/min into the nebulizer (Mira Mist, Perkin Elmer). Argon plasma power was 1400 W, gas flow rates of plasma, nebulizer and auxiliary gas were set to 10 L/min, 0.6 L/min, and 0.2 L/min. Spectral emission at 251.611 nm (Si), 589.292 nm (Na), 213.617 nm (P), and 317.933 nm (Ca) were used. A five point calibration was performed beforehand (standards for ICP, Carl Roth).

Scanning electron microscopy (Gemini Ultra 55, Carl Zeiss). Samples were prepared by embedding powders in conductive paste. Secondary electrons were used for imaging at an accelerating voltage of 2 kV.

Infrared spectroscopy (FTS 3100, Varian). Platelets for transmission measurements (resolution 2 cm^{-1}) were prepared by KBr dilution (1/200 g/g; UVASol, Merck). Base line subtraction was performed manually; reported data is normalized to the maximum absorbance.

X-ray diffraction (D8-Advance, VÅNTEC-1 detector, Bruker AXS). Cu-$K_{\alpha,1}$ radiation ($\lambda = 0.154$ nm) was used in the 2θ range 20° to 55°; step width and counting times were 0.014° and 1.0 s/step.

In vitro bioactivity

Short term *in vitro* bioactivity studies were performed according to Kokubo et al.:[14] 100 mg of the powders were immersed in 50 mL SBF (all purities >99.0%, Sigma Aldrich). The dispersions were kept slightly agitated (120 rpm, Unimax 1010 M, Heidolph Instruments) at 37°C; sampling was performed after 4 h, 8 h, 1 day, 3 days, and 7days. Suspensions were centrifuged (2 min, 2000 rpm), washed with water and acetone and dried (60°C, 24 h).

In vitro biocompatibility

Cell line. *In vitro* cell culture studies were performed using MG-63 osteoblast-like cells (ATCC®, Sigma-Aldrich) isolated from human osteosarcoma. The cells were cultured in Dulbecco's modified Eagle's Medium (DMEM, Gibco®), supplemented with 10 vol % foetal bovine serum (FBS, Sigma-Aldrich) and 1 vol % penicillin and streptomycin (BioChrom) at 37°C in a humidified atmosphere (5% CO_2 in 95% air, Steri-Cycle, Thermo Fisher Scientific). Cell cultures were washed (phosphate-buffered saline PBS, Gibco®) and the growth medium was exchanged every other day. Cell detachment from the well plate was achieved by addition of 3 mL trypsin (Gibco®). Cell stock solutions were obtained by dilution with 7 mL culture medium. Cell concentrations were determined using a Thoma counting chamber. To obtain cell lysate, 1 mL of lysis buffer (Sigma-Aldrich) was added; the cell extracts were centrifuged (2000 rpm, 5 min) after incubation (20 min, 37°C). LDH-activity tests were directly performed; prior to osteoblast activity tests the lysates were stored at −40°C.

TABLE I. Absolute and Relative Compositions of the Powders

	Na_2O/SiO_2 (%)	CaO/SiO_2 (%)	P_2O_5/SiO_2 (%)
BG45S5	56.5 ± 3.9	53.4 ± 3.8	12.5 ± 0.8
BG10	53.6 ± 1.8	56.4 ± 0.7	13.7 ± 4.0
BG30	54.2 ± 1.9	55.9 ± 0.7	13.4 ± 3.9

Given errors calculated by weighted regression and Gaussian error propagation. Absolute composition of BG45S5: 43.6 ± 2.5 wt % SiO_2, 24.6 ± 0.9 wt % Na_2O, 23.3 ± 0.1 wt % CaO, and 5.4 ± 0.1 wt % P_2O_5.

Heat sterilization, cell seeding, and incubation. Sterilization was performed by dry heat (2 h, 160°C). Respective amounts of powders were dispersed directly in the cell growth medium. ZnO (99.9% ZnO, Oxizinc Agalsa) served as negative-control. Particle dispersion was assured by sonification. By inoculation with the prepared cell stock solution, initial cell density was set to 100,000 cells/mL. After cultivation for 48 h and removal of the culture medium the cells were washed twice with PBS.

Cell morphology. Cell morphologies were obtained by bright field microscopy (Eclipse TE 2000-U, Nikon). To observe the formation of cytoskeleton, cell distribution and mineralization in contact with BG particles fluorescence microscopy (FM, DMI 6000B, Leica) was used after staining: After the cultivation period, the adherent cells were fixed with 3.7 vol % paraformaldehyde for 10 min and permeabilised with 0.1 vol % Triton X-100 (in PBS) for 10 min at room temperature. Blue fluorescent DAPI (4′,6-diamidino-2-phenylindole dihydrochloride – Roche) and red fluorescent Alexa Fluor® Phalloidin (Molecular Probes®) were used for cell staining. To detect the cytoskeleton, cells were incubated for 60 min with phalloidin (diluted 1:50 by volume) at room temperature followed by incubation with 1 μg/mL DAPI for 5 min. Mineralization in all the cell culture samples were stained by OsteoImage™ Mineralization Assay (Lonza); stock solution was diluted 1:100 (v/v) and subsequently incubated for 30 min at room temperature. Samples were washed and left in PBS for microscopic imaging.

Lactate dehydrogenase (LDH) activity. The cell proliferation studies 140μL of the lysat were carried out using the lactate dehydrogenase (LDH) assay. One hundred forty microliters of the lysate was treated with 60 μL of a LDH assay mixture (comprised of 33 vol % of each LDH Assay Substrate Solution, LDH Assay Dye Solution, and LDH Assay Cofactor Solution, Sigma-Aldrich). After 30 min incubation in the dark the reaction was stopped by addition of 300 μL hydrochloric acid (1M, Sigma Aldrich). After dilution (400 μL, H_2O) concentrations were determined by absorption measured at 490 nm and 690 nm (UV/Vis-spectrometer, Specord 40, Analytik Jena).

Mitochondrial activity. Cellular viability was characterized by their mitochondrial activity using the WST-8 assay. After incubation, 200 μL of a mixture comprised of 1 vol % WST-8 reagent (Sigma-Aldrich) and 99 vol % cell culture medium

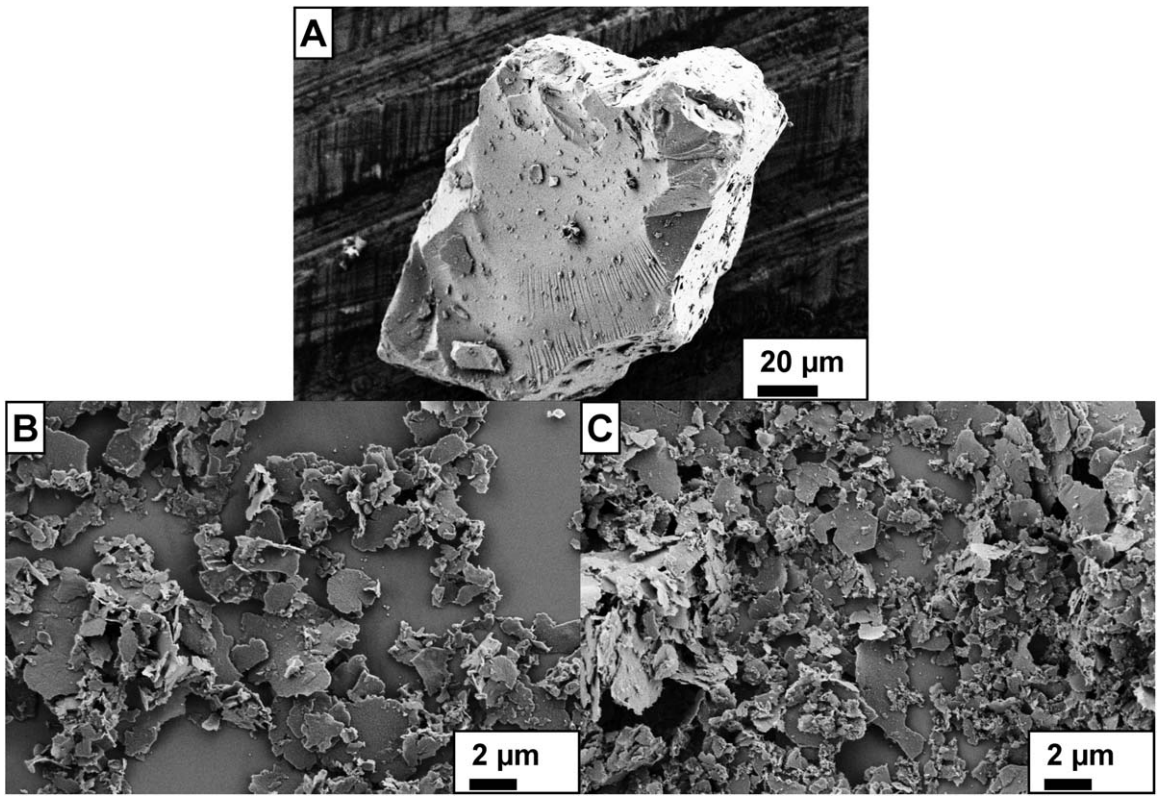

FIGURE 1. SEM images of BG45S5 (A), BG10 (B), and BG30 (C).

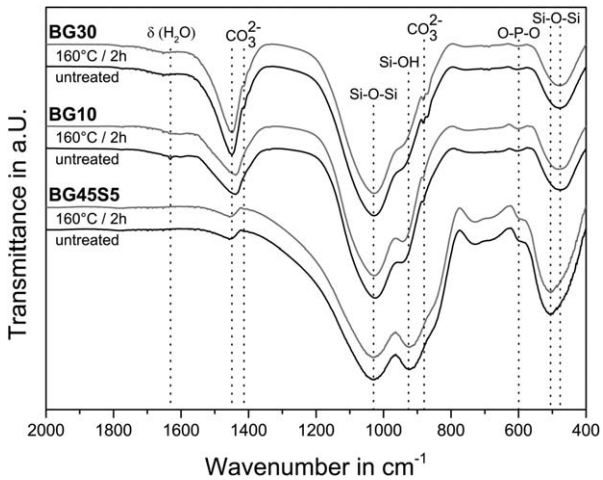

FIGURE 2. FT-IR spectra for BG45S5 (bottom), BG10 (middle) and BG30 (top) before (black lines) and after (grey lines) heat sterilization.

was added to the washed cultures. The resulting mixtures were incubated for additional 90 min in the CO_2-incubator. Concentration determinations were performed by absorption measurements at 450 nm.

Osteoblast activity (ALP). To calculate specific ALP activity, ALP test protein concentrations were determined by a Bradford test (Sigma-Aldrich, Germany): 50 μL of suspended lysates were added to 1.5 mL Bradford reagent; concentration measurements were performed by absorption measurements at 595 nm. To perform the basic ALP activity test 250 μL of centrifuged (5 min, 2000 rpm) lysates were mixed with 100 μL of ALP buffer reagent (0.1*M* tris(hydroxyl-methyl)amino-methane, 2 m*M* magnesium chloride, 9 m*M* *p*-nitrophenylphosphate buffer (*p*-NPP-buffer; pH 9.8)). After incubation (190 min, 37°C), the reaction was stopped by adding 300 μL of NaOH (1 *M*, Sigma Aldrich). After dilution (350 μL H_2O) concentrations were determined by absorption measurements at 405 nm and 690 nm.

Statistical data treatment. Mean values and deviations are derived from four single measurements. For normalization of activities and concentrations the incubation without powder addition is used. Statistical significance (one-way variance analysis ANOVA, Origin 8.5, OriginLab) is marked as significant *($p < 0.05$), very significant **($p < 0.01$), or highly significant ***($p < 0.001$).

RESULTS AND DISCUSSION

Materials characterization

In total, three different powders were investigated for this study: the as-received 45S5BG, BG10 and BG30. Specific surface areas (three independent measurements each) were determined to below 1 m^2/g (45S5BG), to 9.7 ± 1.3 m^2/g (BG10) and to 28.9 ± 0.8 m^2/g (BG30). Static light scattering for BG45S5 (Mastersizer 2000, Malvern Instruments, UK) yielded $x_{50,3} = 21.6$ μm and $x_{90,3} = 100.1$ μm as mass-specific particle diameters of the feed material. The elemental composition of classical 45S5 BG was confirmed for all investigated powders. Concentrations of the submicron glasses normalized to their respective SiO_2 content are given in Table I.

Typical morphologies of the powders are depicted in Figure 1: as-received BG45S5 consists of sharp shards with smooth surfaces (Figure 1A, top); both comminuted powders exhibit flake-like morphologies (Figure 1B and C, bottom—left and right). The lateral extension of the flakes is found in the submicron to the lower micron range. Remarkably, flake thickness accounted for only some tens of nanometers. The amorphous nature of the investigated powders was confirmed by XRD.

A detailed characterization was achieved by FT-IR spectroscopy. As can be seen in Figure 2, comminution leads to only slight variations in composition (black lines); heat further heat sterilization leaves the material unchanged (grey lines). Main changes are surface carbonate formation in course of processing: the feature at 1460 cm^{-1}, at ~1410 cm^{-1} (BG10), 880 cm^{-1} (BG30), and 870 cm^{-1} (BG10 and BG30) evidence surface carbonate coordinated to various

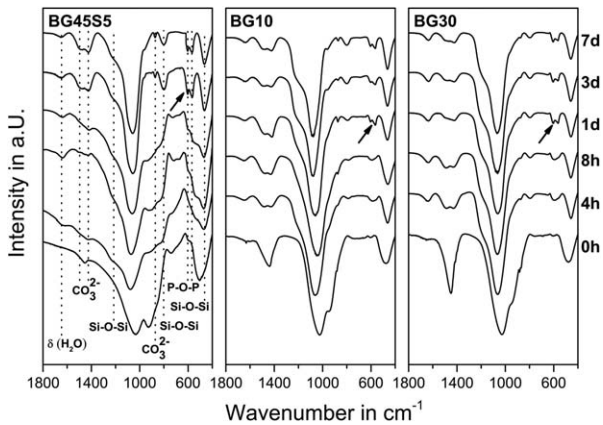

FIGURE 3. FT-IR spectra during SBF of BG45S5 (left), BG10 (middle) and BG30 (right). Crystalline HCAp surface layers are identified by the vibrational modes at 600 cm^{-1} and 570 cm^{-1}; first appearance is marked by the black arrows.

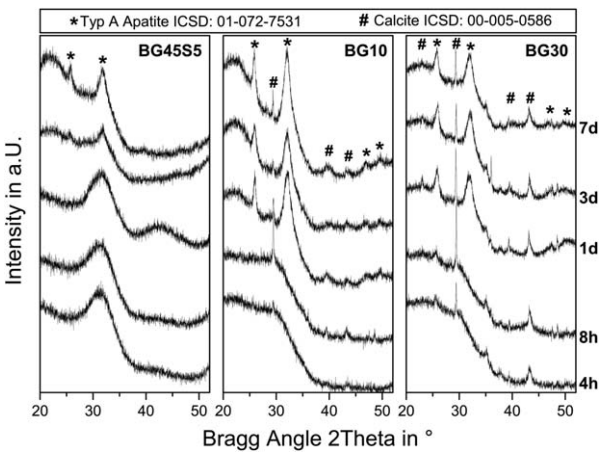

FIGURE 4. X-ray patterns for BG45S5, BG10 and BG30 in course of SBF immersion. Crystalline apatite is found after 3 days for BG45S5 and 1d for both BG10 and BG30.

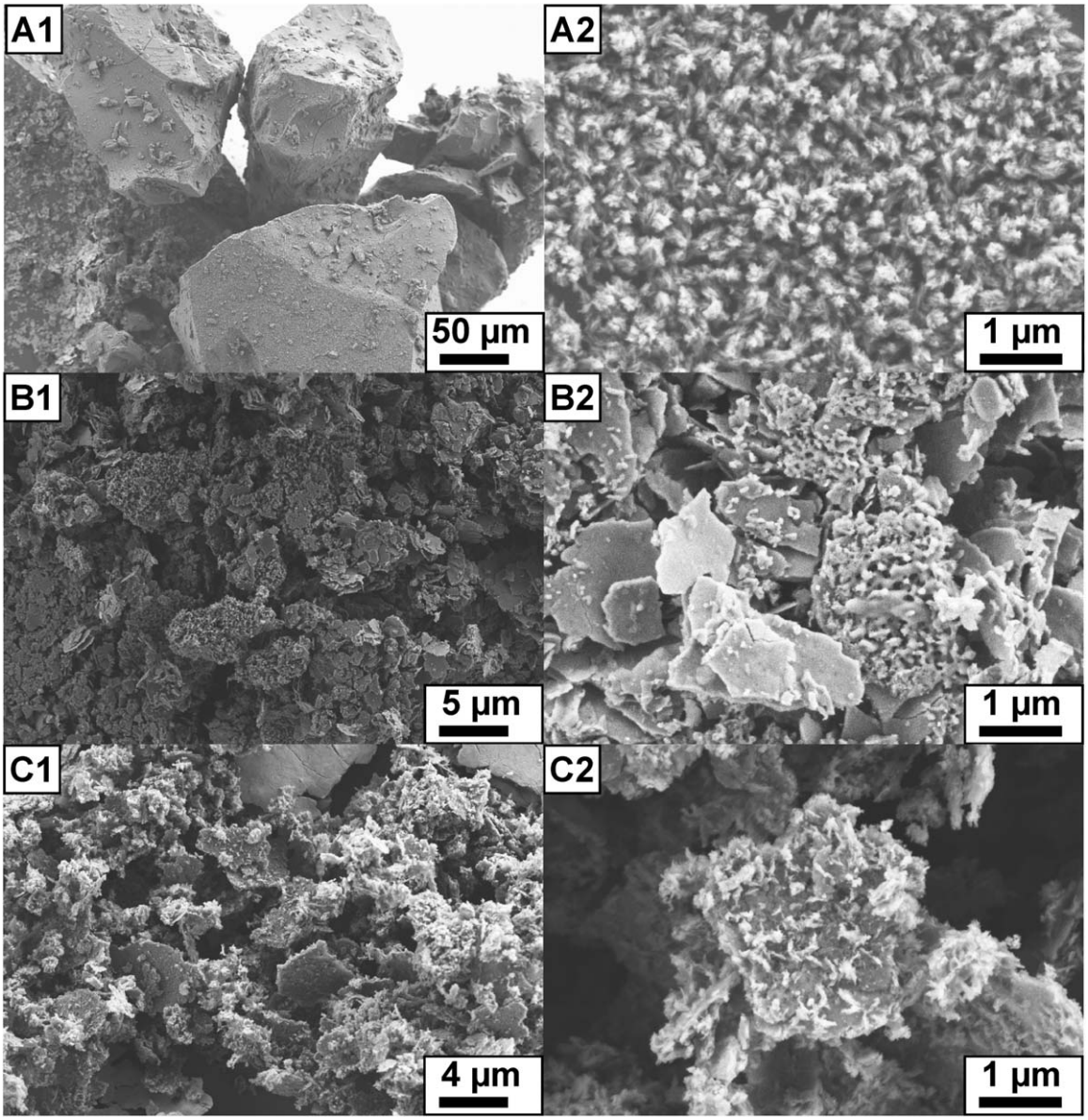

FIGURE 5. SEM Images for BG45S5 (A1-2), BG10 (B1-2) and BG30 (C1-2) after SBF immersion for 7 days (BG45S5) or 1 day (BG10 and BG30).

metallic centres.[33–35] Furthermore, the transmittance at 925 cm^{-1} (nonbridging oxygen groups[36] is increased and the symmetric Si-O-Si vibration shift towards lower wavenumbers[36,37] indicating migration and loss of network modifying ions.

The features at approximately 1026 cm^{-1} and 925 cm^{-1} are caused by overlapping modes from Si-O and P-O bonds.[37] As described above, all powders were found X-ray amorphous and their relative compositions are constant.

Acellular *in vitro* bioactivity tests

In vitro acellular bioactivity was judged by formation of crystalline HCAp in SBF. In Figure 3 IR spectra obtained after various immersion times are depicted. Although the underlying mechanism towards HCAp formation is found identical for the glasses, the respective reaction times differ strongly: HCAp is detected (features at 600 cm^{-1} and 570 cm^{-1}, black arrows) after 1 day only for the comminuted glasses BG10 and BG30; clear signs of HCAp formation for BG45S5 occur after three days. Before splitting amorphous phosphate layers are detected by a rather broad feature at $\sim$590 cm^{-1}.

The splitting of the feature caused by surface carbonate groups initially found at 1460 cm^{-1} into two new features at 1490 cm^{-1} and 1420 cm^{-1} after 4 h (both BG10 and BG30) and 3 days (BG45S5) is in good accordance: splitting occurs both due to transformation of surface carbonates into crystalline carbonates[33] and the substitution of apatite phosphate groups by carbonate groups.[38] Although the presented data is not suited for quantification, maxima in

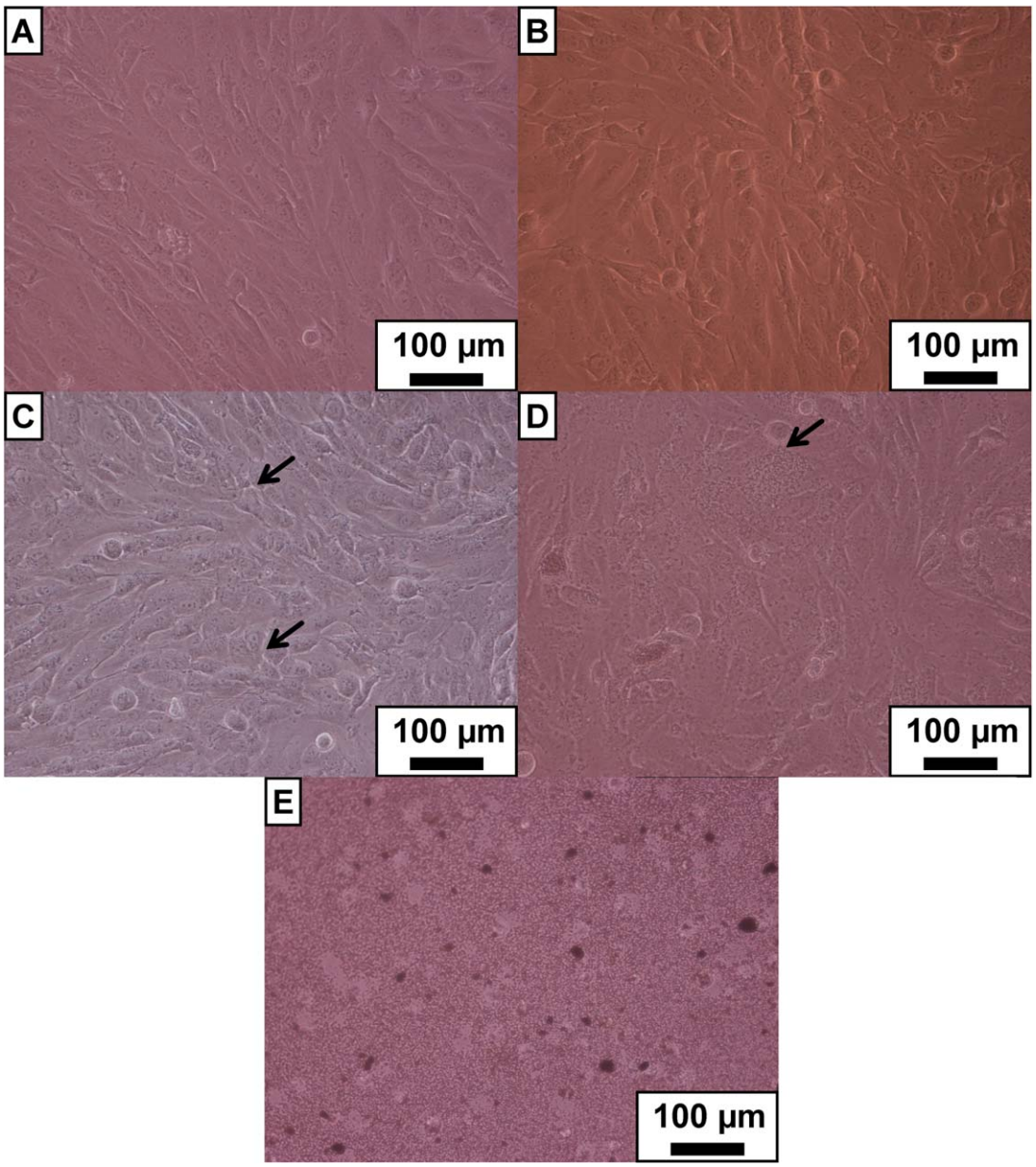

FIGURE 6. Light microscope images of MG-63 cells incubated for 48 h (A) without BG; (B) with BG45S5 (100 µg/mL); (C) with BG10 (100 µg/mL); (D) with BG30 (100 µg/mL); (E) with ZnO (100 µg/mL). [Color figure can be viewed in the online issue, which is available at wileyonlinelibrary.com.]

absorbance of the new features are found after 1 day for BG10 and 8 h for BG30. Constant powder masses were immersed, that is, the observed differences are attributed to the increase in specific surface area.

The formation of carbonates and substitution in HCAp crystals cannot be separated on basis of IR data alone. Therefore X-ray analysis was performed. For identification of HCAp (ICSD—01-072-7531) the [002] reflex (2θ = 25.9°) and the overlap of several peaks in the 2θ range 31.7° to 32.0° can be used. Crystalline calcite (ICSD—00-005-0586) is characterized by its intensive [104] reflex (2θ = 29.4°). As can be seen in Figure 4, crystalline HCAp is clearly found after 1 day for the submicron glasses and 7 days for the as-received glass. In accordance to previous literature reports,[17] carbonate formation is increased for BG10 and BG30: calcite is found after 8 h for BG10 and already after 4h for BG30. In course of the ongoing immersion calcite is dissolved again and scattered intensity drops.

SEM images depicted in Figure 5 revealed that nucleation of presumably HCAp (based on IR and X-ray data) was evenly distributed over the particle surfaces only for BG45S5 (Figure 5—A1, A2). For BG10 (Figure 5—B1, B2) and BG30 (Figure 5—C1, C2) platelet-shaped particles are found covered by precipitates. Our *in vitro* SBF findings clearly show in agreement to previous literature reports[17,39]

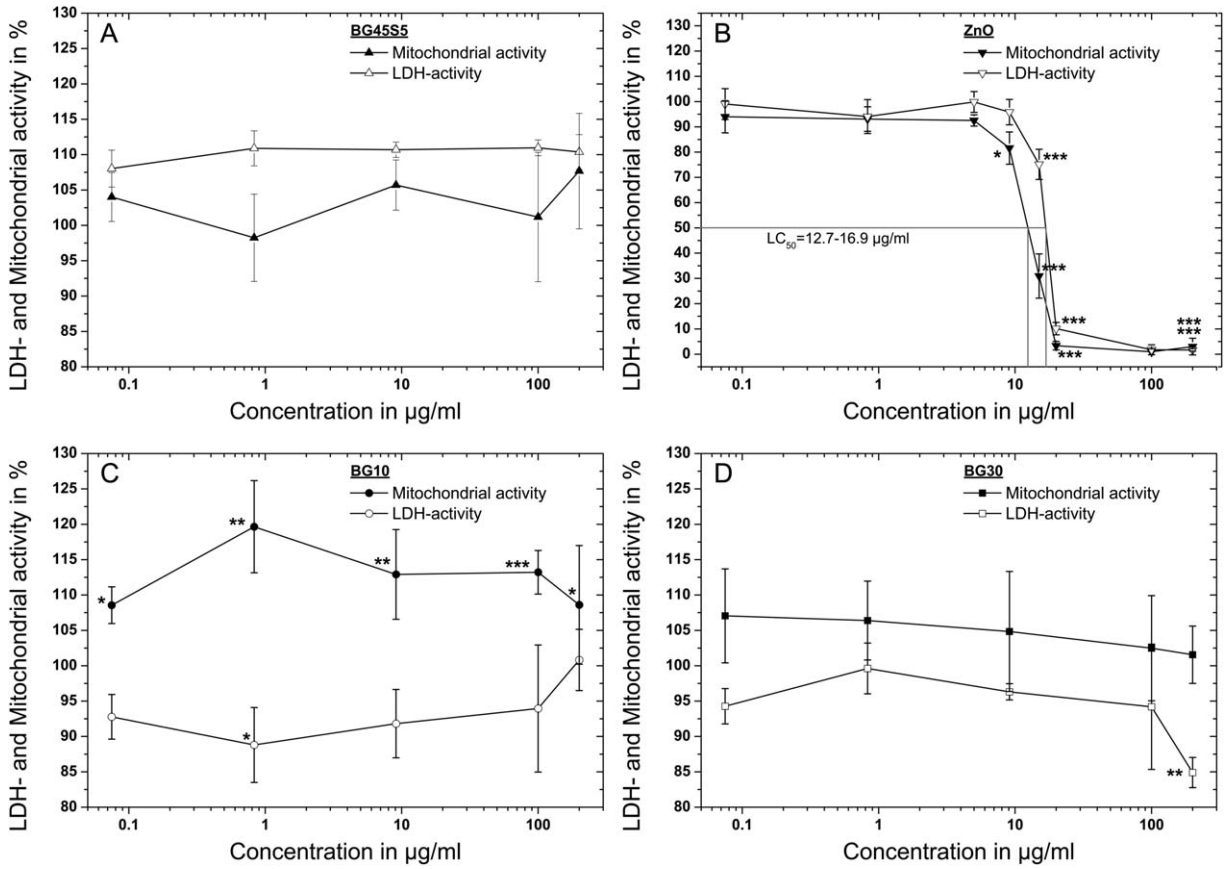

FIGURE 7. LDH and mitochondrial activity of MG-63 cells after incubation for 48 h with varying concentrations (0–200 µg/mL) of (A) BG45S5, (B) ZnO, (C) BG10, and (D) BG30; significance levels: $*p < 0.05$, $**p < 0.01$, $***p < 0.001$.

that bioactivity, in terms of HCAp detection, is enhanced by the increased specific surface area.

In vitro biocompatibility tests

Cell morphology. Cell morphology can serve as a first judgment of biocompatibility. Especially cell toxicity can be easily spotted: upon cell death, the elongated and flattened osteoblast-like MG-63 cells, a sign for biocompatibility of a material,[40,41] are desorbed and the dead cells floating in the medium are characterized by their spherical morphology. Further morphological changes occur if the cells differentiate to osteoblasts and during cell division. Figure 6(b–d) displays representative light micrographs of MG-63 cells incubated for 48 h in the presence of the tested powders (100 µg/mL). The incubation without addition of powder [Figure 6(a)] and the incubation in presence of 100 µg/mL cell-toxic ZnO [Figure 6(e)—particles marked by the arrow] serve as references. Upon incubation with ZnO no living cells were observable. In contrast, all other samples show a dense monolayer of cells [Figure 6(a–d)]. The vast majority of the cells adheres to surfaces and exhibits a characteristic elongated spindle-like morphology. The cells even grow in direct contact to the submicron bioactive glass particles [e.g. Figure 6(d), marked by an arrow]. A comparison of cell coverage yields that the densest layer is obtained during incubation with BG10 [Figure 6(c)], followed by BG30 [Figure 6(d)], BG45S5 [Figure 6(b)] and the reference [Figure 6(a)]. It can be concluded that no cell toxic effect is caused even by the administered high concentrations of BG particles. Especially for BG10 differentiated cells resulting in osteoblasts (marked by arrows) are observed. Some dead cells found in all samples are attributed to natural cell death.

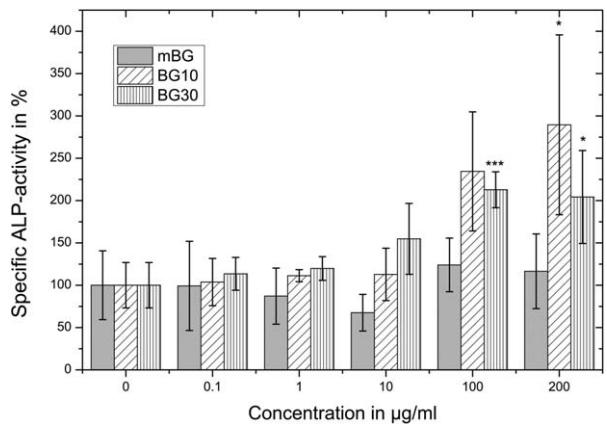

FIGURE 8. Specific ALP activity of MG-63 cells after an incubation for 48 h with various powder amounts (0–200 µg/mL) of BG45S5, BG10 and BG30; significance levels: $*p < 0.05$, $**p < 0.01$, $***p < 0.001$.

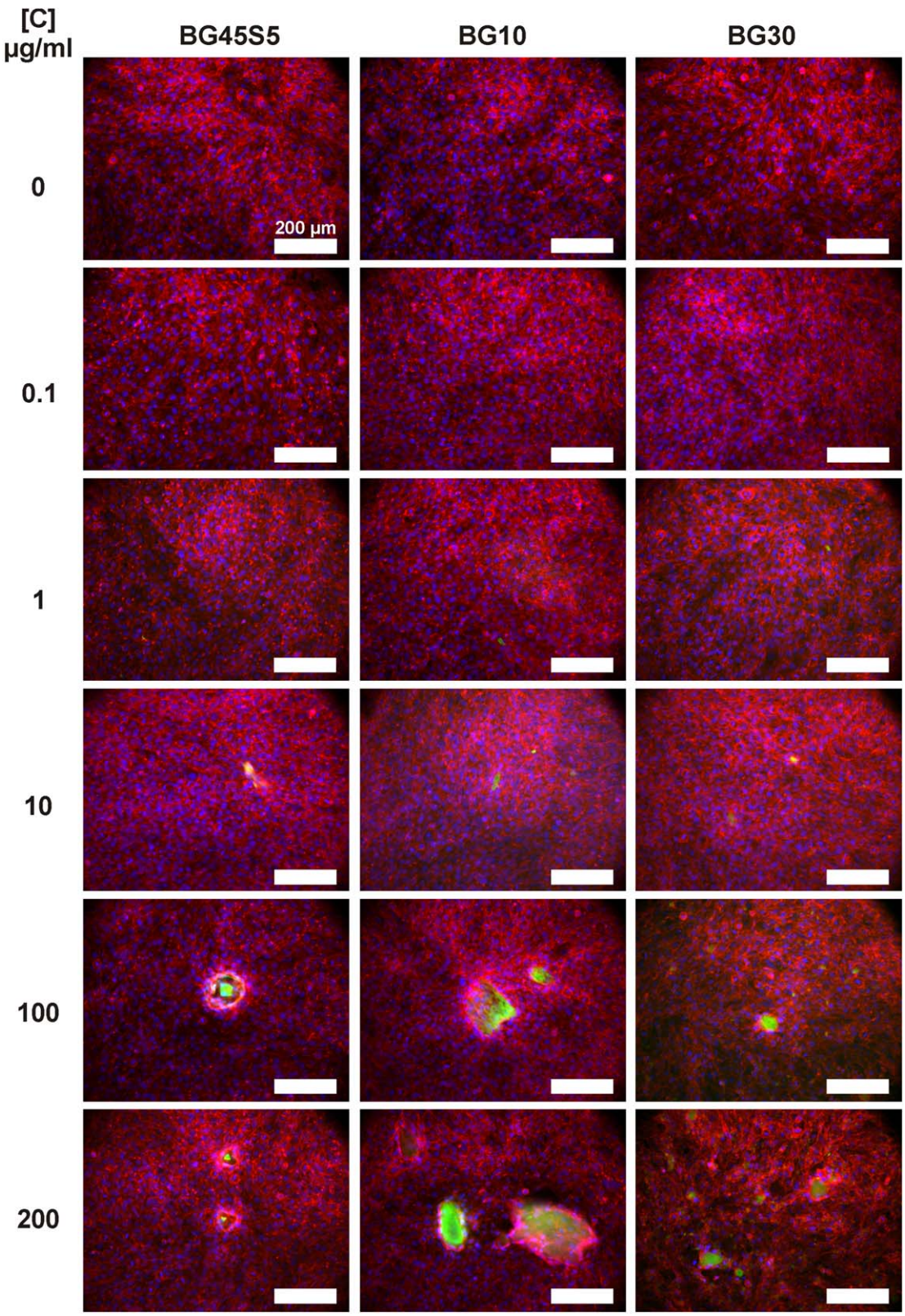

FIGURE 9. Fluorescence microscope images of MG-63 cells incubated for 2 days with different concentrations of BG45S5, BG10, and BG30. Cytoskeleton in red, nucleus in blue, and formed hydroxyapatite in green. Scale bars: 200 µm. [Color figure can be viewed in the online issue, which is available at wileyonlinelibrary.com.]

LDH- and mitochondrial activity. LDH-activity quantification kit was used to quantify cell number by the LDH enzyme activity in cell lysate. Furthermore, the mitochondrial activity was applied to assess the cell viability. The lethal ZnO concentration LC_{50} of the negative control was determined in good accordance to literature reports[42,43] to be 12.7 to 16.9 μg/mL. As can be seen in Figure 7 only slight influences on the cells are observed: The submicron powders seemingly stimulate mitochondrial activity and suppress LDH-activity; activities ranging from 85% to 120% were found in all cases and therefore cell toxicity can be excluded.

Osteoblast activity. Specific ALP-activities of the different cultures differ strongly. As can be seen in Figure 8, the application of BG45S5 does not show a significant influence. In contrast the specific ALP-activities of cells incubated with the submicron powders (at high glass concentrations) are significantly increased. It has to be pointed out that this increase of specific ALP activity at such short incubation periods (48 h) is extraordinary. In contrast to other osteosarcoma cell lines ALP activities of MG-63 cells are usually not influenced by any administered biomaterial within the first 4 d of incubation.[8,44] Previous experiments performed on nBG particles[17] yielded similar trends; however, the specific ALP activity of 300% found in the present experiments for a particle concentration of 200 μg/mL has not been reported.

High ALP activities are favourable: incubation with BG particles could result in an enhancement of biomineralization and to increased hydroxyapatite formation; a rapid bone growth can thus be expected.[8,44]

To further evaluate morphology and mineralization of cells in contact with the BG powders, fluorescence microscope images were taken after staining. In Figure 9 representative images of MG-63 cells incubated at different concentrations of μBG, BG10 and BG30 after 48 h of incubation are shown, whereby the cytoskeleton was stained in red, the nucleus in blue and the formed hydroxyapatite in green. In accordance with Figure 6, on all samples dense monolayers with cell-cell contacts are visible. Compared to the reference (0 μg/mL) sample, MG-63 cells expressed a typical osteoplastic phenotype on all samples. Cytoskeleton staining shows clearly smooth and flat formed extensive actin fibres in MG-63 cells on all samples investigated. Furthermore, MG-63 cells partially exhibit a rounded morphology as discussed above. With help of the green staining, it is possible to visualize hydroxyapatite formation on the BG-particles. In contrast to the low BG concentrations, first mineralization spots could be detected at concentrations of 1 μg/mL BG. At higher concentration (100–200 μg/mL) of BG, mineralization is clearly shown. Interestingly, there are differences in the application of BG particles: MG-63 cells grow on and onto the mineral layer in the BG10 and BG30 samples, whereas a distance ring is formed around the mineralised micro-sized BG particles. As discussed above, FT-IR (Figure 3) and XRD (Figure 4) revealed the formation of HCAp after 1 day of incubation for BG10 and BG30 while for BG45S5 HCAp forms after 3 days of incubation in SBF.

CONCLUSIONS

Bioactivity and biocompatibility of two submicron BG powders obtained by a top-down approach using stirred media mills have been assessed in this study; the as-received powder was used as a reference. The mass specific surface areas of the two obtained submicron powders of flake-like morphology accounted for approximately 10.0 m^2/g (BG10) and 30 m^2/g (BG30); an increase by a factor of 10 and 30 compared to the feed material was realized. As a consequence, increased *in vitro* biocompatibility was found upon immersion in SBF: crystalline hydroxyapatite was already detected after 1 day; 3 days were needed in case of the as-received micron sized BG. Moreover, we have shown *in vitro* biocompatibility by incubating MG-63 cells with various amounts of the three tested glasses; even at the highest studied concentrations (200 μg/mL) no cell toxic effects were found. On the contrary, high concentrations of submicron particles had a significant stimulating effect on the cells: for BG10 a threefold increase in osteoblast activity compared to the as-received micron sized powder was found. The morphology and mineralization of the MG-63 cells in contact with the BG powders were evaluated by fluorescence microscopy after staining: first mineralization spots could be detected at concentrations of 1 μg/mL BG; at higher concentration of BG, mineralization is clearly shown. Whereas MG-63 cells grew directly on and onto the mineral layer for BG10 and BG30 samples, a kind of distance ring was formed for the micro-sized BG particles. Our study thus shows that submicron BG particles produced by a wet milling process are potential candidates for applications in bone tissue engineering and as bone filling materials.

ACKNOWLEDGMENTS

Dr. I. Thompson (King's College London, UK) is kindly acknowledged for supplying the melt derived bioactive glass powder. The authors acknowledge J. Hum and A. Grünewald for experimental assistance.

REFERENCES

1. Hench LL. Biomaterials: A forecast for the future. Biomaterials 1998;19:1419–1423.
2. Jones JR. Review of bioactive glass: From Hench to hybrids. Acta Biomater 2013;9:4457–4486.
3. Hench LL, Splinter RJ, Allen WC, Greenlee TK. Bonding mechanisms at the interface of ceramic prosthetic materials. J Biomed Mater Res 1971;5:117–141.
4. Hench LL. The story of bioglass. J Mater Sci: Mater Med 2006;17: 967–978.
5. Wilson J, Pigott GH, Schoen FJ, Hench LL. Toxicology and biocompatibility of bioglasses. J Biomed Mater Res 1981;15:805–817.
6. Hench LL, Paschall HA. Direct chemical bond of bioactive glass-ceramic materials to bone and muscle. J Biomed Mater Res 1973; 7:25–42.
7. Hench LL. Bioceramics. J Am Ceram Soc 1998;81:1705–1728.
8. Xynos ID, Hukkanen MVJ, Batten JJ, Buttery LD, Hench LL, Polak JM. Bioglass® 45S5 stimulates osteoblast turnover and enhances

bone formation in vitro: Implications and applications for bone tissue engineering. Calcif Tissue Int 2000;67:321–329.
9. Gorustovich AA, Roether JA, Boccaccini AR. Effect of bioactive glasses on angiogenesis: A review of in vitro and in vivo evidences. Tissue Eng Part B: Rev 2010;16:199–207.
10. Ogino M, Ohuchi F, Hench LL. Compositional dependence of the formation of calcium phosphate films on bioglass. J Biomed Mater Res 1980;14:55–64.
11. Kitsugi T, Yamamuro T, Nakamura T, Higashi S, Kakutani Y, Hyakuna K, Ito S et al. Bone bonding behavior of three kinds of apatite containing glass ceramics. J Biomed Mater Res 1986;20: 1295–1307.
12. Filgueiras MR, La Torre G, Hench LL. Solution effects on the surface reactions of a bioactive glass. J Biomed Mater Res 1993;27: 445–453.
13. Kokubo T, Kushitani H, Sakka S, Kitsugi T, Yamamuro T. Solutions able to reproduce in vivo surface-structure changes in bioactive glass-ceramic A-W. J Biomed Mater Res 1990;24:721–734.
14. Kokubo T, Takadama H. How useful is SBF in predicting in vivo bone bioactivity. Biomaterials 2006;27:2907–2915.
15. Chen QZ, Thompson ID, Boccaccini AR. 45S5 Bioglass-derived glass-ceramic scaffolds for bone tissue engineering. Biomaterials 2006;27:2414–2425.
16. Boccaccini AR, Erol M, Stark WJ, Mohn D, Hong Z, Mano JF. Polymer/bioactive glass nanocomposites for biomedical applications: A review. Compos Sci Technol 2010;70:1764–1776.
17. Mačković M, Hoppe A, Detsch R, Mohn D, Stark WJ, Spiecker E, Boccaccini AR. Bioactive glass (type 45S5) nanoparticles: In vitro reactivity on nanoscale and biocompatibility. J Nanopart Res 2012;14.
18. Vollenweider M, Brunner TJ, Knecht S, Grass RN, Zehnder M, Imfeld T, Stark WJ. Remineralization of human dentin using ultrafine bioactive glass particles. Acta Biomater 2007;3:936–943.
19. Gubler M, Brunner TJ, Zehnder M, Waltimo T, Sener B, Stark WJ. Do bioactive glasses convey a disinfecting mechanism beyond a mere increase in pH? Int Endod J 2008;41:670–678.
20. Ostomel TA, Shi Q, Tsung C, Liang H, Stucky GD. Spherical bioactive glass with enhanced rates of hydroxyapatite deposition and hemostatic activity. Small 2006;2:1261–1265.
21. de Zheng H, Wang YJ, Yang CR, Chen XF, Zhao NR. Investigation on the porous biomaterial for bone reconstruction with addition of bio-mimetic nano-sized inorganic particles. KEM 2007;336–338: 1534–1537.
22. Esfahani SI, Tavangarian F, Emadi R. Nanostructured bioactive glass coating on porous hydroxyapatite scaffold for strength enhancement. Mater Lett 2008;62:3428–3430.
23. Zhang Y, Venugopal JR, El-Turki A, Ramakrishna S, Su B, Lim CT. Electrospun biomimetic nanocomposite nanofibers of hydroxyapatite/chitosan for bone tissue engineering. Biomaterials 2008;29: 4314–4322.
24. Couto DS, Zhongkui H, Mano JF. Development of bioactive and biodegradable chitosan-based injectable systems containing bioactive glass nanoparticles. Acta Biomater 2009;5:115–123.
25. Bergmann C, Lindner M, Zhang W, Koczur K, Kirsten A, Telle R, Fischer H. 3D printing of bone substitute implants using calcium phosphate and bioactive glasses. J Eur Ceram Soc 2010;30:2563–2567.
26. Li R, Clark AE, Hench LL. An investigation of bioactive glass powders by sol-gel processing. J Appl Biomater 1991;2:231–239.
27. Brunner TJ, Grass RN, Stark WJ. Glass and bioglass nanopowders by flame synthesis. Chem Commun 2006;13:1384–1386.
28. Knieke C, Romeis S, Peukert W. Influence of process parameters on breakage kinetics and grinding limit at the nanoscale. AICHE J 2011;57:1751–1758.
29. Schmidt J, Plata M, Tröger S, Peukert W. Production of polymer particles below 5μm by wet grinding. Powder Technol 2012;228: 84–90.
30. Damm C, Körner J, Peukert W. Delamination of hexagonal boron nitride in a stirred media mill. J. Nanopart Res 2013;15.
31. Romeis S, Hoppe A, Eisermann C, Schneider N, Boccaccini AR, Peukert W. Enhancing in vitro bioactivity of melt derived 45S5 Bioglass® by comminution in a stirred media mill. J Am Ceram Soc 2013. DOI: 10.1111/jace.12615.
32. Brunauer S, Emmett PH, Teller E. Adsorption of gases in multimolecular layers. J Am Chem Soc 1938;60:309–319.
33. Cerruti M, Morterra C. Carbonate formation on bioactive glasses. Langmuir 2004;20:6382–6388.
34. Miller FA, Wilkins CH. Infrared spectra and characteristic frequencies of inorganic ions. Anal Chem 1952;24:1253–1294.
35. Miller FA, Carlson GL, Bentley FF, Jones WH. Infrared spectra of inorganic ions in the cesium bromide region (700–300 cm−1). Spectrochim Acta 1960;16:135–235.
36. Bunker BC, Tallant DR, Headley TJ, Turner GL, Kirkpatrick RJ. The structure of leached sodium borosilicate glass. Phys Chem Glasses 1988;29:106–120.
37. Cerruti M, Bianchi CL, Bonino F, Damin A, Perardi A, Morterra C. Surface modifications of bioglass immersed in TRIS-buffered solution. A multitechnical spectroscopic study. J Phys Chem B 2005;109:14496–14505.
38. Koutsopoulos S. Synthesis and characterization of hydroxyapatite crystals: A review study on the analytical methods. J Biomed Mater Res 2002;62:600–612.
39. Sepulveda P, Jones JR, Hench LL. Characterization of melt-derived 45S5 and sol-gel-derived 58S bioactive glasses. J Biomed Mater Res 2001;58:734–740.
40. Shapira L, Halabi A. Behavior of two osteoblast-like cell lines cultured on machined or rough titanium surfaces. Clin Oral Implants Res 2009;20:50–55.
41. Hattar S, Berdal A, Asselin A, Loty S, Greenspan DC, Sautier J. Behaviour of moderately differentiated osteoblast-like cells cultured in contact with bioactive glasses. Eur Cell Mater 2002;4:61–69.
42. Brunner TJ, Wick P, Manser P, Spohn P, Grass RN, Limbach LK, Bruinink A et al. In vitro cytotoxicity of oxide nanoparticles: Comparison to lasbestos, silica, and the effect of particle solubility. Environ Sci Technol 2006;40:4374–4381.
43. Lai JCK, Lai MB, Jandhyam S, Dukhande VV, Bhushan A, Daniels CK, Leung SW. Exposure to titanium dioxide and other metallic oxide nanoparticles induces cytotoxicity on human neural cells and fibroblasts. Int J Nanomedicine 2008;3:533–545.
44. Saldaña L, Bensiamar F, Boré A, Vilaboa N. In search of representative models of human bone-forming cells for cytocompatibility studies. Acta Biomater 2011;7:4210–4221.